OPTICAL AND MICROPHYSICAL PROPERTIES OF UPPER CLOUDS MEASURED WITH THE RAMAN LIDAR AND HYDROMETEOR VIDEOSONDE

Tetsu Sakai[(1)], Narihiro Orikasa[(1)], Tomohiro Nagai[(1)], Masataka Murakami[(1)], Kenichi Kusunoki[(1)], Kazumasa Mori[(1)(2)], Akihiro Hashimoto[(3)], Takatsugu Matsumura[(4)], and Takashi Shibata[(5)]

[(1)]*Meteorological Research Institute, 1-1 Nagamine, Tskuba, Ibaraki 305-0052, Japan, tetsu@mri-jma.go.jp, norikasa@mri-jma.go.jp, tnagai@mri-jma-go.jp, mamuraka@mri-jma.go.jp, kkusunok@mri-jma.go.jp*
[(2)] *Present affiliation: Japan Meteorological Agency, 1-3-4 Otemachi, Chiyoda-ku, Tokyo 100-8122, Japan, kmori@met.kishou.go.jp*
[(3)]*Advanced Earth Science and Technology Organization, MRI, 1-1 Nagamine, Tskuba, Ibaraki 305-0052, Japan, ahashimo@mri-jma.go.jp*
[(4)]*Japan Science and Technology Agency, MRI, 1-1 Nagamine, Tskuba, Ibaraki 305-0052, Japan, takatsugum@hotmail.com*
[(5)]*Graduate School of Environmental Studies, Nagoya University, Furo-cho Chikusa-ku, Nagoya 464-8601, Japan, shibata_takashi@nagoya-u.jp*

ABSTRACT

Optical and microphysical properties of the upper clouds at an altitude range of 5–11 km were measured over Tsukuba, Japan on 29–30 March 2004 using a Raman lidar and a balloon-borne hydrometeor videosonde (HYVIS). The HYVIS measurement showed that the cloud particles were ice crystals whose shapes were columnar, bullet-like, plate-like, and irregular with 7–400 μm in size. The Raman lidar measurement showed that the depolarization ratio ranged from 0 to 35% and the extinction-to-backscatter ratio (lidar ratio) ranged from 0.3 to 30 sr at 532 nm for the clouds. The comparison between the measured data and theoretical calculations of the cloud optical properties suggests that the observed variations in the depolarization ratio and lidar ratio were primarily due to the variation in the proportion of the horizontally oriented ice crystals in the clouds.

1. INTRODUCTION

Cirrus clouds frequently appear in the upper troposphere and can affect the Earth's climate. They can affect the radiation balance by scattering and absorbing the solar and terrestrial radiation and can affect the water and material cycles through precipitation processes [1, 2]. In order to understand the effects of the clouds on these processes, it is necessary to measure the temporal and spatial distributions of the cloud microphysical properties such as phase, shape, size, number concentration, orientation, and the optical properties. Lidar is a useful tool for measuring the vertical distribution of the optical properties of the cirrus clouds. However, we have little knowledge about the relation between the optical properties obtainable using the lidar and the in-situ cloud microphysical properties.

To study the relation between the optical and microphysical properties, a measurement of the upper clouds using the Raman lidar and balloon-borne hydrometeor videosonde (HYVIS) was carried out over Tsukuba, Japan, on 29–30 March 2004. This paper reports the preliminary results of a comparison between cloud properties measured for the first time using the Raman lidar and HYVIS. A more detailed analysis of the measured data is given by [3].

2. INSTRUMENTATIONS

2-1. Raman lidar

We used the Raman lidar developed by the Meteorological Research Institute (MRI), Japan. The details of the lidar system and data analysis procedure are described by [4]. The lidar transmits laser pulses at a wavelength of 532 nm vertically into the atmosphere and collects the inelastically backscattered (Raman backscattered) light by the nitrogen molecules at 607 nm and the water vapor at 660 nm as well as the elastically backscattered (Mie and Rayleigh backscattered) light by the cloud/aerosol particles and molecules at 532 nm using Cassegrainian telescopes. The lidar was vertically pointing in this study.

The derived parameters are the backscattering ratio (R), particle backscattering coefficient (β), extinction coefficient (α), depolarization ratio (δ), lidar ratio (S), and the water vapor mixing ratio (w). The relative humidity was calculated from the lidar-derived w and the radiosonde-derived temperature and pressure. The vertical resolution of the analyzed data was 197 m and the temporal resolution was 9 min except in the case of the high-resolution data of R and δ, shown in Figs. 1a and 1b with resolutions 96 m and 3 min. The uncertainty in the analyzed data was calculated using Poisson statistics for the observed photon counts.

2-1. Hydrometeor videosonde (HYVIS)

The hydrometeor videosonde (HYVIS) measures the vertical distributions of the in-situ microphysical properties of cloud particles by taking microscopic images using the CCD video cameras on board the balloon. The details of the HYVIS are described by [5, 6]. The dimensions of the HYVIS instrument are 280 ×

106 × 500 mm, and its weight is approximately 2.4 kg. All the instruments are on board a balloon. The HYVIS collects cloud particles through an inlet that is 1 cm in diameter with a suction fan and samples them on the surface of a transparent 35 mm leader film coated with silicon oil. Microscopic images of the particles are taken using two small video cameras with different magnifications. The detectable particle size range is 7 μm – 5 mm in the maximum dimension. The images are transmitted in real time to a ground receiver by 1687-MHz microwaves. The microphysical properties obtainable from the cloud microscopic images are the particle shape, size, and the number concentration. These properties were analyzed manually. The temporal resolution of the data is approximately 10 s, which corresponds to the vertical resolution of approximately 67 m (ascending speed of the balloon with an average of 6.7 m s^{-1} in this study).

In addition to the HYVIS, the balloon measured the atmospheric pressure, temperature, and relative humidity using radiosonde (RS-01G, Meisei Electronic Co., ltd.). Further, a chilled mirror hygrometer (SnowWhite, meteolabor AG), on board the same balloon, measured the dew/frost points.

3. RESULTS

3-1. Lidar data

Fig. 1 shows the vertical and temporal cross section of R, δ, S, α, and the relative humidity with respect to ice (RHi) obtained by the Raman lidar for the period 1802–0009 LST on 29–30 March 2004. Data with measurement uncertainties less than 10% for δ, 50% for S and RHi, and 100% for R and α are plotted in the figure. For the α and S values, the multiple scattering effect is not considered. The cross section of R (Fig. 1a) shows high values (>10) for an altitude range of 6–11 km. The values of δ (Fig. 1b) were mostly 20–35% for an altitude range of 5–11 km except for the middle altitude region (6.5–8 km), indicating the predominance of randomly oriented large nonspherical particles in that region. These particles were ice crystals as revealed by the HYVIS measurement (Fig. 2). The values of S were mostly between 0.3 sr and 30 sr in that region. These values of δ and S are consistent with those reported by the previous measurements of cirrus clouds [4, 7, 8] and those calculated theoretically for the ice crystals [9, 10]. It should be noted that these values showed low values (δ < 10% and S < 10 sr) in the middle of the cloud (6.5–8 km in altitude). This was possibly due to the presence of horizontally oriented ice crystals that will be discussed in subsection 3-3. The value of α in the cloud varied between 0.02 and 1.54 km^{-1} (Fig. 1d), and the apparent optical thickness varied between 0.3 and 2.6. The relative humidity was saturated or slightly supersaturated with respect to ice (≥100%) in the lower part of the clouds (Fig. 1e), which supports the presence of the ice crystals.

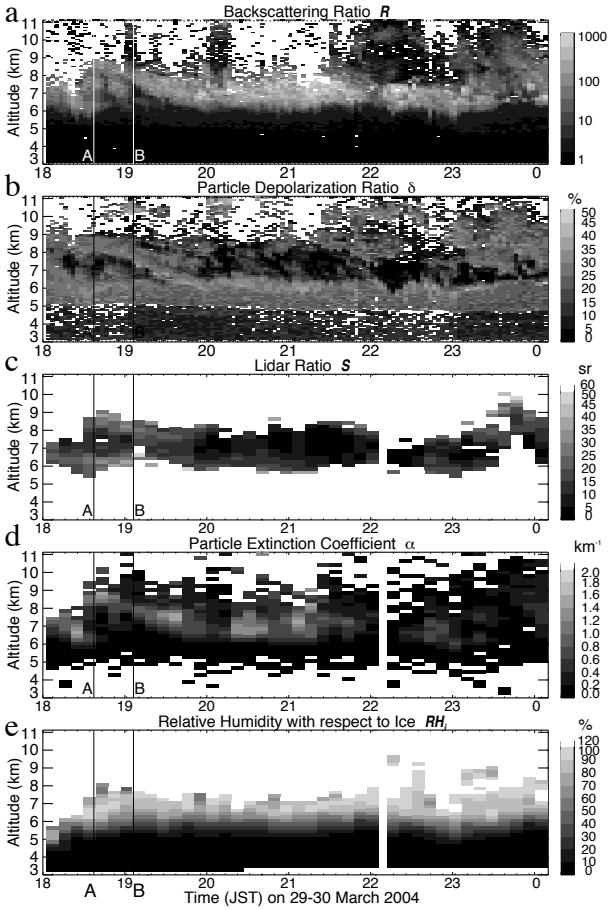

Fig. 1. Temporal and vertical cross section of the backscattering ratio (a), particle depolarization ratio (b), lidar ratio (c), extinction coefficient (d) and relative humidity with respect to ice (e) obtained using the Raman lidar for 29–30 March 2004 over Tsukuba. The vertical lines in the figures denote the times when the HYVIS-mounted balloon was launched (A) and reached an altitude of 12 km (B). The data with large uncertainties due to the weak signal intensity were not shown.

3-2. HYVIS data

Fig. 2 shows the examples of microscopic images of the cloud particles taken by the HYVIS at altitudes of 8.8, 8.4, and 7.8 km. The temperatures at the three altitudes were –39.3, –36.7, and –33.8 degrees, and RHi values at these altitudes were 106%, 96%, and 99% measured with chilled mirror hygrometer. Fig. 2 shows that ice crystals were predominant at the three altitudes. The shape of the crystals was mostly columnar, bullet-like, plate-like, and irregular. The crystal size (maximum dimension) was in the range of 7–400 μm and the mean particle size generally increased with decreasing height. The maximum size was 100–200 μm in the upper altitude region (8.25–11.5 km, Figs. 2a and 2b) and 250–400 μm in the lower region (6.0–8.25 km, Fig. 2c). The total particle number concentration ranged between

1–496 L^{-1} at altitudes between 5.0 and 11.5 km and was the highest at 8.25–8.5 km (Fig. 2b). It should be noted that few water droplets were detected with HYVIS. This result suggests that the ice crystals were predominant in the cloud and they produced the lidar-observed variations in δ and S, which is discussed in the following subsection.

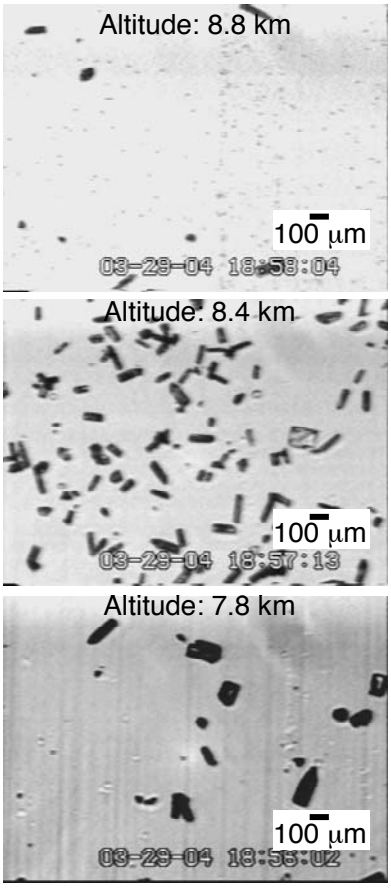

Fig. 2. Examples of microscopic images of the cloud particles taken using the HYVIS at altitudes of 8.8 km (a), 8.4 km (b), and 7.8 km (c) over Tsukuba on 29 March 2004.

3-3. Relation between depolarization ratio and lidar ratio

The lidar measurement showed that the values of δ and S varied as 0–35% and 0.3–30 sr in the clouds (Figs. 1b and 1c). In order to study the observed variations of these values, we compare them with those calculated theoretically for the cloud particles. The result of the comparison is shown in Fig. 3 by the scatter plot of δ as a function of S. The lidar-observed values are shown for the cloud data taken between altitudes of 6.4–8.4 km for the period 1847–0009 LST (total 280 data points). The average uncertainties of the data are 0.2% for δ and 2 sr for S. The theoretical values are shown for the three cloud particles: 1) randomly oriented hexagonal ice columns whose prism-to-basal face axis ratio (c/2a) ranges from 1.25 to 5.9 calculated using the geometrical ray-tracing technique [10]; 2) horizontally oriented ice crystals calculated using the geometrical ray-tracing technique [11], T-matrix method [12], and the finite difference time domain method [13]; and 3) water droplets (C1 model [14]) calculated using the Mie theory. In the case of the randomly oriented ice columns, the surface roughness was accounted by statistical deviations of ray paths during the ray-tracing in the crystals; each time a ray hits a crystal surface, the normal to this surface is tilted with respect to its original direction by a certain angle and also rotated around it. The tilt angle is randomly distributed between zero and one degree, whereas the azimuth angle is randomly distributed between zero and 180 degree. The calculated values for the randomly oriented ice columns ranged from δ = 33% and S = 12 sr (c/2a = 1.25) to δ = 32% and S = 38 sr (c/2a = 5.9). The theoretically calculated values of δ and S for the other randomly oriented ice crystal shapes (plate-, bullet rosette-, dendrite-, and aggregate-like) are similar (δ = 22–36% and S = 6–19 sr) to these values except for highly distorted crystals, hollow columns, and small (a few micrometers) crystals that show high S values (>70 sr) [10, 15].

Fig. 3 shows that the lidar-observed δ values decreased with decreasing values of S. Moreover, most of these values lie within the area enclosed by the triangle whose two vertices represent the theoretical values for the randomly oriented ice crystals with c/2a = 1.25 (δ = 33% and S = 12 sr) and c/2a = 5.9 (δ = 32% and S = 38 sr), and the third vertex of this triangle represents the values for the horizontally oriented ice crystals (δ = 0% and S < 1 sr). This result suggests that the ice crystals were predominant in the observed cloud and that the proportion of the horizontally oriented crystals in the randomly oriented crystals varied therein. There are few measurement data showing values close to that for water droplets (δ = 0% and S = 18 sr), suggesting that there were no regions wherein water droplets were predominant. This result is consistent with the results of the HYVIS measurement (e.g., Fig. 2) that showed that the water droplets were nearly absent for the detected size range (>7 μm). The vertical variations of δ and S (Figs. 1b and 1c) showed that these values were the lowest (δ < 10% and S < 10 sr) in the middle of the clouds (6.5–8 km in altitude), suggesting that the proportion of the horizontally oriented crystals was the largest in that region. However, we cannot verify this estimation about the crystal orientation using the HYVIS data because the HYVIS cannot measure the particle orientation without disturbing it during the sampling process. To verify the ice crystal orientation, it is useful to measure the δ of the clouds by tilting the lidar away from the vertical direction in order [16, 17].

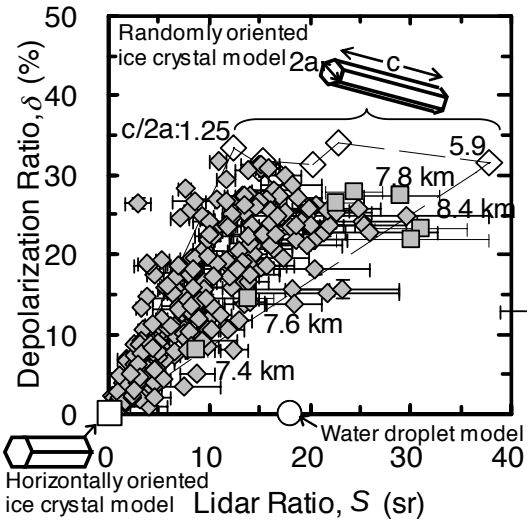

Fig. 3. Scatter plot of the particle depolarization ratio (δ) as a function of the lidar ratio (S) for the clouds. Solid diamonds represent the lidar-derived values. Open symbols show the theoretical values for the randomly oriented hexagonal columns with aspect ratio between 1.25 and 5.9 (open diamonds), horizontally oriented ice crystal (open square), and water droplets (open circle).

4. CONCLUSION

The result of the upper cloud measurements using the Raman lidar and HYVIS and the comparison with theoretical calculations suggest that the lidar-observed variations in δ and S were primarily due to the variation in the proportion of the horizontally oriented ice crystals in the clouds. The result obtained suggests that by measuring S and δ with the lidar, it is possible to distinguish the phase and orientation of the cloud particles: randomly oriented ice crystals, horizontally oriented ice crystals, and water droplets. This information is useful for evaluating the radiative effect of the clouds because it critically depends on the phase and the crystal orientation [9, 18]. However, this method should be verified by measuring ice clouds by tilting the lidar and by measuring mixed-phase clouds with the lidar and HYVIS or other in-situ instruments.

REFERENCES

1. Liou K. N., Influence of cirrus clouds on weather and climate processes: A global perspective, *Mon. Wea. Rev., 114*, 1167–1198, 1986.

2. Stephens G. L., Cirrus, climate, and global change. *Cirrus*, D. Lynch, K. Sassen, D. O'C. Starr, and G. L. Stephens, Eds., Oxford University Press, 433–448, 2002.

3. Sakai T., N. Orikasa, T. Nagai, M. Murakami, K. Kusunoki, K. Mori, A. Hashimoto, T. Matsumura, and T. Shibata, Optical and microphysical properties of upper clouds measured with the Raman lidar and hydrometeor videosonde: A case study on 29 March 2004 over Tsukuba, Japan. *J. Atmos. Sci.,* 2006 (accepted).

4. Sakai T., T. Nagai, M. Nakazato, and T. Matsumura, Ice clouds and Asian dust studied with lidar measurements of particle extinction-to-backscatter ratio, particle depolarization, and water vapor mixing ratio over Tsukuba, *App. Opt., 42*, 7103–7116, 2003.

5. Murakami M., and T. Matsuo, Development of the hydrometeor videosonde, *J. Atmos. Oceanic Tech., 7*, 613–620, 1990.

6. Orikasa N., and M. Murakami, A new version of hydrometeor videosonde for cirrus cloud observations, *J. Meteorol. Soc. Japan, 75*, 1033–1039, 1997.

7. Ansmann A., U. Wandinger, M. Riebesell, C. Weitkamp and W. Michaelis, Independent measurement of extinction and backscatter profiles in cirrus cloud by using a combined elastic-backscatter lidar, *Appl. Opt., 31*, 7113–7131, 1992.

8. Sassen K., and S. Benson, A midlatitude cirrus cloud climatology from the Facility for Atmospheric Remote Sensing: II. Microphysical properties derived from lidar depolarization, *J. Atmos. Sci., 58,* 2103-2112, 2001.

9. Takano Y., and K. N. Liou, Solar radiative transfer in cirrus clouds. Part II: theory and computation of multiple scattering in an anisotropic medium, *J. Atmos. Sci., 46,* 20–36, 1989.

10. Hess M., R. B. A. Koelemeijer, and P. Stammes, Scattering matrices of imperfect hexagonal ice crystals, *J. Quant. Spectrosc. Radiat. Transfer*, *60*, 301–308, 1998.

11. Liou K. N., and H. Lahore, Laser sensing of cloud composition: A backscattered depolarization technique, *J. Appl. Meteorol., 13,* 257–263, 1974.

12. Mishchenko M. I., D. J. Wielaard, and B. E. Carlson, T-matrix computations of zenith-enhanced lidar backscatter from horizontally oriented ice plates, *Geophys. Res. Lett., 24*, 771–774, 1997.

13. Yang P., Y. X. Hu, D. M. Winker, J. Zhao, C. A. Hosteller, B. A. Baum, M. I. Mishchenko, and J. Reichardt, Enhanced lidar backscattering by horizontally oriented ice plates, *J. Quant. Spectrosc. Radiat. Transfer*, 79-80, 1139–1157, 2003.

14. Deirmendjian D., *Electromagnetic Scattering on Spherical Polydispersions*, Elsevier, 78, 1969.

15. Yang P., and K. N. Liou, Finite difference time domain method for light scattering by nonspherical and nonhomogeneous particles. *Light Scattering by Nonspherical Particles*, M. I. Mishchenko, J. W. Hovenier, and L. D. Travis, Eds., Academic Press, 173–221, 2000.

16 Platt C. M. R., Lidar backscatter from horizontal ice crystals plates, *J. Appl. Meteorol., 17*, 482–488, 1978.

17. Thomas L., J. C. Cartwright, and D. P. Wareing, Lidar observations of the horizontal orientation of ice crystals in cirrus clouds, *Tellus, 42B*, 211–216, 1990.

18. Asano S., Transfer of solar radiation in optically anisotropic ice clouds, *J. Meteorol. Soc. Japan*, 61, 402–413, 1983.